J Comput Neurosci (2016) 40:347–362
DOI 10.1007/s10827-016-0601-0

Impact of slow K^+ currents on spike generation can be described by an adaptive threshold model

Ryota Kobayashi[1,2] · **Katsunori Kitano**[3]

Received: 26 February 2015 / Revised: 6 March 2016 / Accepted: 1 April 2016 / Published online: 16 April 2016

Abstract A neuron that is stimulated by rectangular current injections initially responds with a high firing rate, followed by a decrease in the firing rate. This phenomenon is called spike-frequency adaptation and is usually mediated by slow K^+ currents, such as the M-type K^+ current (I_M) or the Ca^{2+}-activated K^+ current (I_{AHP}). It is not clear how the detailed biophysical mechanisms regulate spike generation in a cortical neuron. In this study, we investigated the impact of slow K^+ currents on spike generation mechanism by reducing a detailed conductance-based neuron model. We showed that the detailed model can be reduced to a multi-timescale adaptive threshold model, and derived the formulae that describe the relationship between slow K^+ current parameters and reduced model parameters. Our analysis of the reduced model suggests that slow K^+ currents have a differential effect on the noise tolerance in neural coding.

Keywords Spike generation mechanism · Slow K^+ currents · Conductance-based models · Integrate-and-fire models · Model reduction

Action Editor: J. Rinzel

✉ Ryota Kobayashi
r-koba@nii.ac.jp

[1] Principles of Informatics Research Division, National Institute of Informatics, 2-1-2 Hitotsubashi, Chiyoda-ku, Tokyo, Japan

[2] Department of Informatics, SOKENDAI (The Graduate University for Advanced Studies), 2-1-2 Hitotsubashi, Chiyoda-ku, Tokyo, Japan

[3] Department of Human and Computer Intelligence, Ritsumeikan University, 1-1-1 Nojihigashi, Kusatsu, Shiga 525-8577, Japan

1 Introduction

Neuronal adaptation is the change in the responsiveness of a neuron over time. Adaptation may play an important role in the extraction of important information from an ever-changing environment and is the product of several factors, including ion channels, synapses, and network dynamics. In this study, we focus on adaptation at the single neuron level. When a neuron is stimulated by rectangular current injections, it initially responds with a high firing rate, followed by a decrease in the firing rate. This phenomenon is called spike-frequency adaptation and is observed in most pyramidal neurons in various brain areas. The spike-frequency adaptation is usually mediated for by M-type K^+ current (I_M) (Brown and Adams 1980; Adams et al. 1982), Ca^{2+}-activated K^+ current (I_{AHP}) (Brown and Griffith 1983; Madison and Nicoll 1984), Na^+-activated K^+ current (Schwindt et al. 1989), or the slow inactivation of Na^+ current (Fleidervish et al. 1996; Kim and Rieke 2003). In terms of the spike-frequency adaptation generated by slow K^+ currents, conductance-based models including slow K^+ channels have been studied. These models can reproduce the electrophysiological properties of a neuron (see Koch 1999 for a review) and provide insights into the underlying biophysical mechanisms.

Studies using the conductance-based models have suggested that the distinct biophysical mechanisms responsible for the spike-frequency adaptation have different impacts on neural coding (Ermentrout et al. 2001; Prescott and Sejnowski 2008). For example, I_M improves spike-timing coding, whereas I_{AHP} improves spike-rate coding (Prescott and Sejnowski 2008). These results indicate that specific biophysical mechanisms underlying adaptation may impact the coding properties of

a neuron. On the other hand, due to the complexity of the detailed models, it remains unclear how the kinetics of slow K^+ currents influence the spike generation mechanism.

In order to understand the spike generation mechanism, it is essential to reduce the detailed neuron models to simplified models. There have been many attempts to simplify the detailed models (Ermentrout and Kopell 1986; Abbott and Kepler 1990; Destexhe 1997; Kistler et al. 1997; Richardson et al. 2003; Fourcaud-Trocmé et al. 2003 for review Rinzel and Ermentrout 1998; Gerstner and Kistler 2002; Izhikevich 2007). A direct approach to obtain the reduced model is to fit the simplified model to simulated data set generated by the detailed model. This approach has clarified the underlying mechanism of spike generation, such as, integration properties (Kistler et al. 1997; Jolivet et al. 2004), adaptation (Brette and Gerstner 2005), and spike threshold variability (Kobayashi and Shinomoto 2007). However, this approach cannot predict the effect of the detailed model parameters (physiological parameters) on spike generation. Another approach is to develop a mathematical framework to simplify the detailed models. For example, the FitzHugh–Nagumo model and integrate-and-fire models (Gerstner and Kistler 2002) were derived from the Hodgkin–Huxley model (Abbott and Kepler 1990; Richardson et al. 2003).

In this study, we extend the mathematical reduction approach by including the spike history effect that is essential to describe the impact of slow K^+ currents on spike generation. We show that the detailed conductance-based neuron model can be reduced to a multi-timescale adaptive threshold model (Kobayashi et al. 2009; Yamauchi et al. 2011), and derive the formulae that describe the relationship between the slow K^+ current parameters and the reduced model parameters. We evaluate the reduced model by predicting spike trains of the detailed model. Finally, we examine the effect of noise on the coding property of a neuron using the reduced model.

2 Materials and methods

2.1 Single neuron models

2.1.1 Conductance-based model

We analyzed a single-compartment conductance-based model based on a model for the cerebral cortex and thalamic neurons proposed by Pospischil et al. (2008), that was extended to include Ca^{2+}-activated K^+ (AHP) current (Mainen and Sejnowski 1996; Tsubo et al. 2004). The membrane voltage V of a neuron is described by the following equation:

$$C_m \frac{dV}{dt} = -I_L - I_{Na} - I_{Kd} - I_M - I_{Ca} - I_{AHP} + I_{\mathrm{ex}}, \tag{1}$$

where C_m is the membrane capacitance and I_{ex} is the external input current. The ionic currents consist of the leak current $I_L = g_L(V - E_L)$, Na^+ current $I_{Na} = g_{Na} m^3 h (V - E_{Na})$, delayed rectifier K^+ current $I_{Kd} = g_{Kd} n^4 (V - E_K)$, muscarinic K^+ current $I_M = g_M p (V - E_K)$, Ca^{2+} current $I_{Ca} = g_{Ca} q^2 r (V - E_{Ca})$, and AHP current $I_{AHP} = g_{AHP} s (V - E_K)$, where g_x and E_x are the maximal ionic conductances and the reversal potentials, respectively. The gating variables $w \in \{m, h, n, p, q, r, s\}$ are described by the Hodgkin − Huxley formalism.

$$\frac{dw}{dt} = \alpha_w\left(V, \left[Ca^{2+}\right]\right)(1-w) - \beta_w\left(V, \left[Ca^{2+}\right]\right)w, \tag{2}$$

where α_w and β_w are the activation and inactivation functions, respectively (see Table 1 for details), and $[Ca^{2+}]$ represents the calcium concentration. The Ca^{2+} concentration is described by (Mainen and Sejnowski 1996; Tsubo et al. 2004)

$$\frac{d\left[Ca^{2+}\right]}{dt} = -10^5 \cdot \frac{I_{Ca}}{2F} - \frac{\left[Ca^{2+}\right] - \left[Ca^{2+}\right]_\infty}{\tau_{Ca}}, \tag{3}$$

where $F = 9.6485 \times 10^4$ [C/mol] is the Faraday constant, $[Ca^{2+}]_\infty = 0.05$ [μM] is the equilibrium concentration, and τ_{Ca} is Ca^{2+} time constant. The slow K^+ current parameters were varied in the ranges $g_M \in [0.05, 0.4]$ [mS/cm^2], $g_{AHP} \in [0.05, 0.4]$ [mS/cm^2], $\tau_{\max} \in [0.5, 4]$ [s], $\beta_s \in [10, 90]$ [/s], and $\tau_{Ca} \in [0.1, 0.9]$ [s]. The remaining parameters are shown in Table 1. This model was solved numerically using the forward Euler integration method with a time step of 0.025 [ms] (Jolivet et al. 2004). We further confirmed that the results were quantitatively the same for a time step of 0.01 [ms].

2.1.2 Adaptive threshold models

The potential u of a model neuron obeys a linear differential equation,

$$\frac{du}{dt} = -\frac{u}{\tau_m} + \frac{I_{\mathrm{ex}}}{C_m}. \tag{4}$$

where τ_m is the membrane time constant. The neuron generates a spike if the potential u reaches the spike threshold $\theta_u(t)$ from below, and the threshold is linearly modulated by spikes (Kobayashi et al. 2009; Yamauchi et al. 2011)

$$\begin{aligned} &\text{If } u(t) > \theta_u(t) \rightarrow \text{Emit a spike at time } t, \\ &\theta_u(t) = \theta_u^\infty + \sum\nolimits_{k:t_k<t} H_u(t - t_k), \end{aligned} \tag{5}$$

where t_k is the k-th spike time, $H_u(t)$ is the threshold kernel that describes the effect of previous spikes, and the sum is taken up

Table 1 Parameters of a detailed conductance-based model

Channel x	Gating variables w	α_w [/ms]	β_w [/ms]	g_x [mS/cm^2]	E_x [mV]
Na	m	$\frac{-0.32(V+45)}{e^{-(V+45)/4}-1}$	$\frac{0.28(V+18)}{e^{(V+18)/5}-1}$	50.0	50.0
	h	$0.128e^{-(V+41)/18}$	$\frac{4}{1+e^{-(V+18)/5}}$	–	–
K	n	$\frac{-0.032(V+43)}{e^{-(V+43)/5}-1}$	$0.5e^{-(V+48)/40}$	5.0	−90.0
M	p	$\frac{p_\infty(V)}{\tau_\infty(V)}$	$\frac{1-p_\infty(V)}{\tau_\infty(V)}$	0.1	−90.0
Ca	q	$\frac{-0.055(V+27)}{e^{-(V+27)/3.8}-1}$	$0.94e^{-(V+75)/17}$	0.001	120
	r	$0.000457e^{-(V+13)/50}$	$\frac{0.0065}{1+e^{-(V+15)/28}}$	–	–
AHP	s	$0.01[Ca^{2+}]$	0.02	0.2	−90.0

The ion channel x, the gating variable w, the activation and inactivation functions α_w and β_w, the maximal conductance g_x, and the reversal potential E_x are summarized. α_p and β_p are given by the equilibrium value p_∞ and the time constant $\tau_p(V)$, $p_\infty(V)=\frac{1.0}{1+e^{\frac{V+35}{10}}}$, $\tau_p(V)=\tau_{max}/\left\{3.3e^{(V+35)/20}+e^{-(V+35)/20}\right\}$

The other parameters are $C_m=1.0$ [μF/cm^2], $g_L=0.1$ [mS/cm^2], $\tau_{max}=1.0$ [s] and $E_L=-80$ [mV], unless otherwise stated

to the most recent spike time. The multi-timescale adaptive threshold (MAT) model (Kobayashi et al. 2009) is a special case of the adaptive threshold model (Eq. (5)). The threshold kernel is given by the sum of exponential functions for each spike in the history,

$$H_u(t)=\begin{cases}0 & (t\le 0)\\ \sum_{j=1}^{L}\alpha_j e^{-t/\tau_j} & (0<t)\end{cases}, \tag{6}$$

where L is the number of exponential functions and α_j and τ_j are the weights and the threshold time constants, respectively.

It is worth noting that the potential u of the adaptive threshold model is different from the voltage of the leaky integrate-and-fire (LIF) model (Gerstner and Kistler 2002). The potential does not reset after a spike and continuously integrates the input current, whereas the voltage in the LIF model is reset after each spike.

2.2 Input currents

We used two types of input current $I_{ex}(t)$. The first input is a constant current with a pulse,

$$I_{ex}(t)=I_c+q_c\delta(t-t_p), \tag{7}$$

where I_c [μ A/cm^2] is the strength of the constant current, q_c [nC/cm^2] and t_p [ms] are the amplitude and timing of the pulse, respectively, and $\delta(t)$ is the Dirac's delta function. The constant part I_c is tuned to maintain the membrane potential at V_c and the pulse amplitude is set to shift the voltage up to −45 [mV], $q_c=C_m(-45-V_c)$. The amplitude should be large enough that the neuron always generates a spike. In all simulations, the neuron was stimulated by the pulse after it achieves the steady state. The second input is an *in vivo*-like current modeled by the Ornstein − Uhlenbeck process (Tuckwell 1988; Kobayashi et al. 2011),

$$\frac{dI_{ex}}{dt}=-\frac{I_{ex}-\mu}{\tau_{syn}}+\sqrt{\frac{2\sigma^2}{\tau_{syn}}}\eta(t), \tag{8}$$

where, μ and σ are the mean and standard deviation (SD) of the input, $\tau_{syn}=2$ [ms] is the synaptic time constant, and $\eta(t)$ is the Gaussian white noise with zero mean and unit variance.

2.3 Calculation of the spike threshold

We evaluated the instantaneous spike threshold of the detailed conductance-based model (Eqs. (1), (2), and (3)). To evaluate the spike threshold at time t_0, i.e., $\theta_V(t_0)$, we stimulate the model neuron with an impulse, $I_{ex}(t)=q\delta(t-t_0)$, and observe whether the model neuron generate a spike or not. The spike threshold is defined as $\theta_V(t_0)=V(t_0-0)+q_{min}$, where $V(t_0-0)$ is the voltage immediately before the pulse injection and q_{min} is the minimal pulse amplitude for generating a spike (Fig. 1).

The minimal amplitude q_{min} can be calculated using the bisection method (Press et al. 2007). Initially, a voltage interval $[a, b]$ is selected such that a (b) is lower (higher) than the spike threshold. The initial interval was set as [−80, 0]. Next, we check whether the midpoint $c=(a+b)/2$ is larger than the spike threshold by observing the voltage for 50 [ms]. If the neuron emits a spike after the voltage shift, c is higher than the threshold and the subinterval $[a, c]$ is selected. Otherwise the subinterval $[c, b]$ is selected. This procedure is repeated until the interval is sufficiently small (less than 10^{-4}).

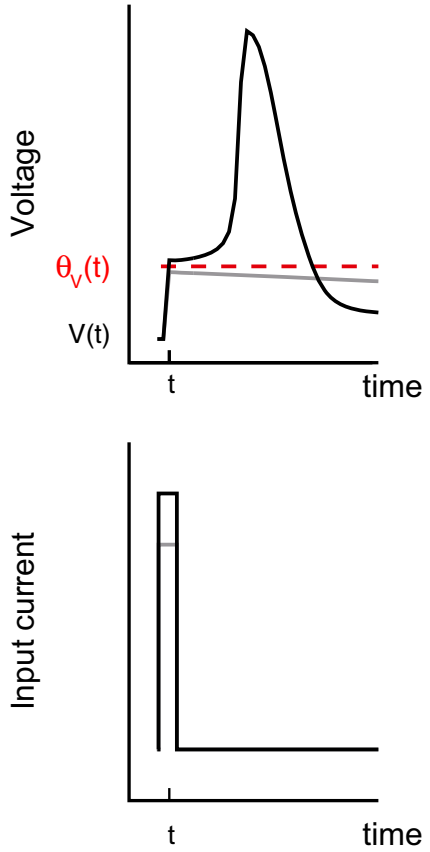

Fig. 1 Calculation of spike threshold of a model neuron. The spike threshold $\theta_V(t)$ is defined as the minimal voltage for generating an action potential (*Top*). The minimal voltage is obtained by applying an impulse to the neuron (*Bottom*)

2.4 Reduction of a conductance-based neuron model

We have developed a reduction procedure from a detailed conductance-based model (Koch 1999; Izhikevich 2007) to an adaptive threshold model. We start from a conductance-based neuron model described by

$$C_m \frac{dV}{dt} = -\sum\nolimits_{\text{ion}} I_{\text{ion}}\left(V, \overrightarrow{w}\right) + I_{\text{ex}}(t), \tag{9}$$

where I_{ion} is an ionic current and $\overrightarrow{w} = (w_1, \cdots, w_d)$ is a vector of gating variables. Each gating variable w_i is described by the kinetic equation (2).

The reduction consists of two approximations. First, we assume that a spike threshold $\theta_V(t)$ is written as:

$$\theta_V(t) = \theta_V^{\infty} + \sum\nolimits_{\text{ion},\ k:t_k<t} h_{\text{ion}}(t-t_k), \tag{10}$$

where θ_V^{∞} is the spike threshold at the resting state and h_{ion} describes the threshold modulation after a spike by an ionic current. If the voltage $V(t)$ exceeds the threshold $\theta_V(t)$, the neuron generates a spike. In addition, it is assumed that the previous spikes affect the spike threshold linearly. The validity of the assumption was tested by the comparison with the spike threshold of the detailed neuron model (data not shown). The effect of the spike waveform is incorporated into the reset rule. If the voltage exceeds the threshold, we shift the time and the voltage: $t \to t + w_{sp}$ and $V \to V + \delta V$, where w_{sp} is the spike width and δV is the voltage change during a spike. Specifically, the spike width w_{sp} is approximately $2 \sim 4$ [ms] and the voltage change δV is $-20 \sim -10$ [mV].

Second, we assumed that the ionic currents I_{ion} are given by the sum of a spike-triggered ionic current $\eta_{\text{ion}}(t)$ and a leak current in the subthreshold regime ($V < \theta_V$):

$$I_{\text{ion}}\left(V, \overline{w}\right) \approx \sum\nolimits_{k:t_k<t} \eta_{\text{ion}}(t-t_k) + \overline{g}_{\text{ion}}(V-E_{\text{ion}}), \tag{11}$$

where $\overline{g}_{\text{ion}}$, E_{ion} are the average conductance and the reversal potential of an ionic current, respectively. By substituting Eq. (11) into (9), we obtain

$$C_m \frac{dV}{dt} = -g_{\text{tot}}(V-E_{\text{tot}}) - \sum\nolimits_{\text{ion},\ k} \eta_{\text{ion}}(t-t_k) + I_{\text{ex}}(t), \tag{12}$$

where $g_{\text{tot}} = \sum_{\text{ion}} \overline{g}_{\text{ion}}$ is the total conductance and $E_{\text{tot}} = \sum_{\text{ion}} \overline{g}_{\text{ion}} E_{\text{ion}} / g_{\text{tot}}$ is the effective reversal potential. The formal solution of Eq. (12) can be written as,

$$\begin{aligned} V(t) = E_{\text{tot}} - C_m^{-1} \sum\nolimits_{\text{ion},\ k} \int_0^{t-t_k} \eta_{\text{ion}}(t-t_k-s) e^{-\frac{s}{\tau_m}} ds \\ + C_m^{-1} \int_0^{t} I_{\text{ex}}(t-s) e^{-\frac{s}{\tau_m}} ds, \end{aligned} \tag{13}$$

where $\tau_m = C_m / g_{\text{tot}}$ is the effective membrane time constant. The Eq. (13) is a special case of the Spike Response Model (SRM) (Kistler et al. 1997; Gerstner and Kistler 2002; Jolivet et al. 2004). Here, the SRM is used to interpret the effect of the ionic currents on spike generation in the conductance-based model.

Let us consider a new variable u that follows a linear equation without resetting after a spike,

$$\frac{du}{dt} = -\frac{u}{\tau_m} + \frac{I_{\text{ex}}}{C_m}, \tag{14}$$

As the solution of Eq. (14) is $u = C_m^{-1} \int_0^t I_{\text{ex}}(t-s) e^{-s/\tau_m} ds$, the relationship between the new variable and the voltage is

$$u = V - E_{\text{tot}} + C_m^{-1} \sum\nolimits_{\text{ion},\ k} \int_0^{t-t_k} \eta_{\text{ion}}(t-t_k-s) e^{-\frac{s}{\tau_m}} ds - \sum\nolimits_k \delta V e^{-\frac{t-t_k-w_{\text{sp}}}{\tau_m}}, \tag{15}$$

where the last term represents the voltage change during a spike. The spike threshold for u can be written as

$$\theta_u(t) = \theta_u^{\infty} + \sum\nolimits_k H(t-t_k), \tag{16}$$

where $\theta_u^{\infty} = \theta_V^{\infty} - E_{\text{tot}}$ and

$$H(t) = -\delta V e^{-\frac{t-w_{\text{sp}}}{\tau_m}} + C_m^{-1} \sum\nolimits_{\text{ion}} \int_0^t \eta_{\text{ion}}(t-s) e^{-\frac{s}{\tau_m}} ds + \sum\nolimits_{\text{ion}} h_{\text{ion}}(t). \tag{17}$$

The effective threshold kernel $H(t)$ is given by the voltage change during a spike, the spike-triggered ionic currents, and the spike threshold variation after a spike.

It should be noted that only the spike-triggered components of the ionic currents are considered in our framework. However, some of these currents, in particular I_M, can be activated at voltages lower than the spike threshold (Prescott and Sejnowski 2008). Thus, the accuracy of the approximation may deteriorate if the voltage fluctuations are large.

2.5 Evaluation of the reduced model

We evaluated the reduced model by predicting the spike train of the detailed model neuron. The predictive performance was evaluated by injecting six fluctuating currents generated by the Ornstein − Uhlenbeck processes (Eq. (8)). The two types of input currents, i.e., the moderately noisy ($\sigma = \mu$) input and the highly noisy ($\sigma = 2\mu$) input, were examined. For each current type, three values of the mean μ were chosen so that the neuron generated spikes with 5, 10, and 20 [Hz]. The input parameters were (μ, σ) = (1.98, 1.98), (2.45, 2.45), (3.24, 3.24), (1.33, 2.66), (1.65, 3.30), and (2.22, 4.44) for the neuron with I_M and (μ, σ) = (1.84, 1.84), (2.15, 2.15), (2.75, 2.75), (1.28, 2.56), (1.58, 3.16), and (2.10, 4.20) for the neuron with I_{AHP}. Two input–output data sets $\{I(t), V(t)\}$ were obtained by injecting two independent fluctuating currents for 50 [s], which were characterized by the same parameters (μ, σ, τ_s), into the detailed model.

The performance was evaluated based on the coincidence factor Γ (Kistler et al. 1997; Jolivet et al. 2004) defined by

$$\Gamma = \frac{N_c - \langle N_c \rangle}{N_d + N_m} \cdot \frac{2}{1 - 2\nu\Delta}, \tag{18}$$

where N_d and N_m are the number of spikes generated by the detailed model and by the reduced model, N_c is the number of coincidences with precision Δ between the two spike trains, $N_c = 2\nu N_d \Delta$ is the expected number of coincidences using the Poisson process with the same rate ν with which the reduced model generates spikes. The coefficient Γ is 1 only if all the spikes coincided within Δ. A homogeneous Poisson process with the firing rate of the detailed model would yield Γ = 0, which is the chance level. The precision Δ was set to 4 [ms] and the spike time of the detailed model is defined as the time when the voltage crosses 0 [mV].

3 Results

3.1 Typical behavior of the detailed conductance-based model

We first observed the behavior of a single-compartment conductance-based model with I_{Na}, I_{Kd}, I_{M}, I_{Ca}, and I_{AHP} (Section 2.1). A rectangular current was injected into the three model neurons, i.e., the neuron with no adaptation ($g_{\text{M}} = g_{\text{AHP}} = 0$ [mS/cm^2]), the neuron with I_{M} ($g_{\text{M}} = 0.1$, $g_{\text{AHP}} = 0$ [mS/cm^2]), and the neuron with I_{AHP} ($g_{\text{M}} = 0$, $g_{\text{AHP}} = 0.2$ [mS/cm^2]).

The neuron with no adaption did not exhibit spike-frequency adaptation, i.e., the firing rate does not decrease during the stimulation (Fig. 2a). By contrast, the neuron with I_{M} or I_{AHP} exhibited spike-frequency adaptation, i.e., the firing rate dropped after the onset of the stimulation (Fig. 2b, c). The firing rate of the neuron with I_{AHP} does not decrease gradually, because the neuron has the s-gate for I_{AHP}. Consistent with previous studies (Benda and Herz 2003; Prescott and Sejnowski 2008), the slow K^+ currents induced spike-frequency adaptation. Due to the complexity and the nonlinearity of the detailed model, it is not clear how slow K^+ currents regulate spike generation of a neuron. Thus, we investigated the effects of slow K^+ currents by mapping the detailed neuron model to a simplified model, and derived a reduced model that clarifies how slow K^+ currents modulate the effective spike threshold.

3.2 Spike triggered ionic current: $\eta_{\text{ion}}(t)$

A constant current with a pulse (Eq. (7)) was injected into the neuron with I_{M} and the neuron with I_{AHP}, and the spike-triggered ionic currents $\eta_{\text{ion}}(t)$ were calculated. Because Na^+, K^+, and Ca^{2+} currents vanish within a brief period immediately after the spike (typically 4 [ms] after the spike onset), we focused on analyzing slow K^+ currents, I_{M} and I_{AHP} (Fig. 3a, b).

First, we examined the spike-triggered current induced by I_{M}, $\eta_{\text{M}}(t)$. By replacing an action potential with a rectangular pulse, similar to the approach of Destexhe (1997), the spike-triggered current can be approximated by the exponential function (Appendix A),

$$\eta_{\text{M}}(t) \approx a_{\text{M}} e^{-t/\tau_p\left(\bar{v}\right)}, \tag{19}$$

where $\tau_p(\bar{v})$ is the p-gate time constant and $\bar{v}$ is an average voltage after a spike. The formula (19) is in

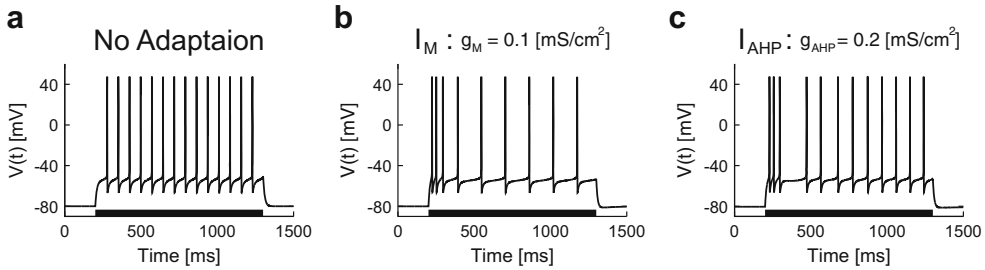

Fig. 2 Response of the detailed neuron model to a rectangular current. A rectangular current was injected into the three detailed neurons, i.e., the neuron with no adaptation (**a**: $g_M = g_{AHP} = 0$ [mS/cm^2]), the neuron with I_M (**b**: $g_M = 0.1$, $g_{AHP} = 0$ [mS/cm^2]), and the neuron with I_{AHP} (**c**: $g_M = 0$, $g_{AHP} = 0.2$ [mS/cm^2]). The stimulus period (200–1300 [ms]) is indicated as a *black bar*. The input current was 2.5 [μA/cm^2] (**a**), 3.2 [μA/cm^2] (**b**), and 3.1 [μA/cm^2] (**c**). The other parameter values are given in Table 1

agreement with $\eta_M(t)$ obtained from the detailed neuron model for various values of I_M parameters (g_M, τ_{max}) and membrane depolarization V_c (Fig. 3c and data not shown for τ_{max} and V_c). There is a slight discrepancy in $\eta_M(t)$ between the detailed model and Eq. (19) for small t, which may be due to the spike waveform. A more accurate formula can be obtained by incorporating this effect (Appendix A).

Second, we examined the spike-triggered current induced by I_{AHP}, $\eta_{AHP}(t)$. By replacing the calcium current

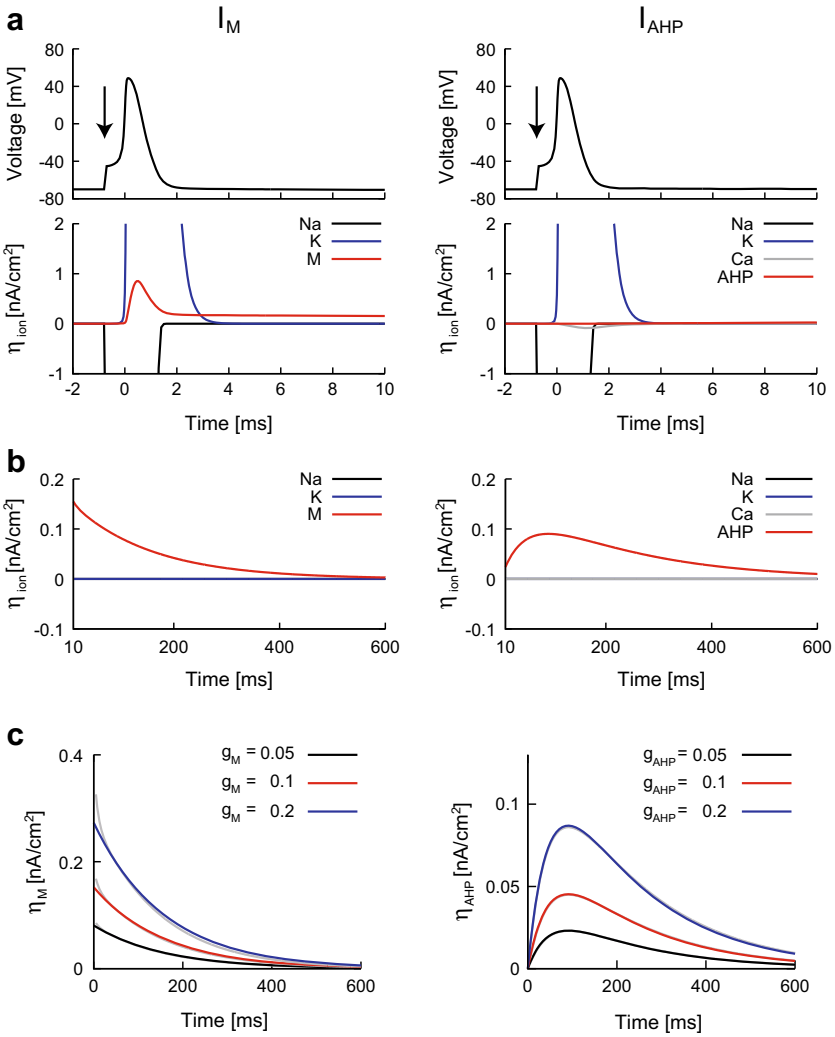

Fig. 3 Effects of slow K^+ currents on the spike-triggered currents. **a**: A constant current with a pulse was injected into the neuron with I_M (left) and the neuron with I_{AHP} (right). *Top and bottom panel* represent the voltage and the spike-triggered currents $\eta_{ion}(t)$ in the vicinity of a spike, respectively. *Arrows* represent the timing of the pulse injection. **b**: Spike-triggered ionic currents after a spike. **c**: Slow spike-triggered currents $\eta_M(t)$ (left, *gray*) and $\eta_{AHP}(t)$ (right, *gray*) were compared to the approximate formulae (Eqs. 19, 20) (*black*, *red*, and *blue*). The maximal conductances (g_M, g_{AHP}) were tested at three levels, i.e., 0.05, 0.1, and 0.2 [mS/cm^2]. The membrane depolarization was $V_c = -70$ [mV], and the other parameter values were given in Table 1

with an impulse, the spike-triggered current can be approximated by the sum of two exponentials (Appendix A).

$$\eta_{\mathrm{AHP}}(t) \approx a_{\mathrm{AHP}} \left(e^{-t/\tau_{\mathrm{Ca}}} - e^{-t/\tilde{\tau}_s} \right), \tag{20}$$

where τ_{Ca} is the Ca^{2+} time constant, $\tilde{\tau}_s = \beta_s^{-1}$ is an approximation of the s-gate time constant, and β_s is the inactivation rate of the s-gate. The formula (20) is also in agreement with $\eta_{\mathrm{AHP}}(t)$ obtained from the detailed neuron model for various values of I_{AHP} parameters (g_{AHP}, β_s, and τ_{Ca}) and the membrane depolarization V_c (Fig. 3c and data not shown for β_s, τ_{Ca} and V_c).

3.3 Spike threshold variation by an ionic current: $h_{\mathrm{ion}}(t)$

A constant current with a pulse (Eq. (7)) was injected into the detailed model neurons and the instantaneous spike threshold was calculated (Section 2.3). Again, three neurons were examined, i.e., the neuron with no adaptation, the neuron with I_{M}, and the neuron with I_{AHP}. Whereas the spike threshold decays rapidly after a spike in the neuron with no adaptation, it decays slowly in the neuron with I_{M} or I_{AHP} (Fig. 4b). We can thus conclude that the threshold variation after a spike is mainly caused by the slow K^+ currents.

The spike threshold variation induced by I_{M} was evaluated by comparing the spike threshold in the neuron with I_{M} to that with no adaptation. The spike threshold variation is approximately proportional to the spike triggered current $\eta_{\mathrm{M}}(t)$ (Appendix B),

$$h_{\mathrm{M}}(t) \approx b_{\mathrm{M}} e^{-t/\tau_p} \left(\bar{v} \right), \tag{21}$$

where the weight b_{M} is proportional to a_{M} in Eq. (19). Equation (21) can accurately describe $h_{\mathrm{M}}(t)$ for various values of the I_{M} parameters (g_{M}, $\tau_{\max}$) and of the membrane depolarization V_c (Fig. 4c and data not shown for $\tau_{\max}$ and V_c). Next, the spike threshold variation induced by I_{AHP} was evaluated by comparing the threshold in the neuron with I_{AHP} to that without I_{AHP}. The spike threshold variation is approximately proportional to the spike triggered current $\eta_{\mathrm{AHP}}(t)$ (Appendix B),

$$h_{\mathrm{AHP}}(t) \approx b_{\mathrm{AHP}} \left(e^{-t/\tau_{\mathrm{Ca}}} - e^{-t/\tilde{\tau}_s} \right), \tag{22}$$

where the weight b_{AHP} is proportional to a_{AHP} in Eq. (20). Equation (22) can accurately describe $h_{\mathrm{AHP}}(t)$ for various values of the I_{AHP} parameters (g_{AHP}, β_s, and τ_{Ca}) and the membrane depolarization V_c (Fig. 4c and data not shown for β_s, τ_{Ca} and V_c).

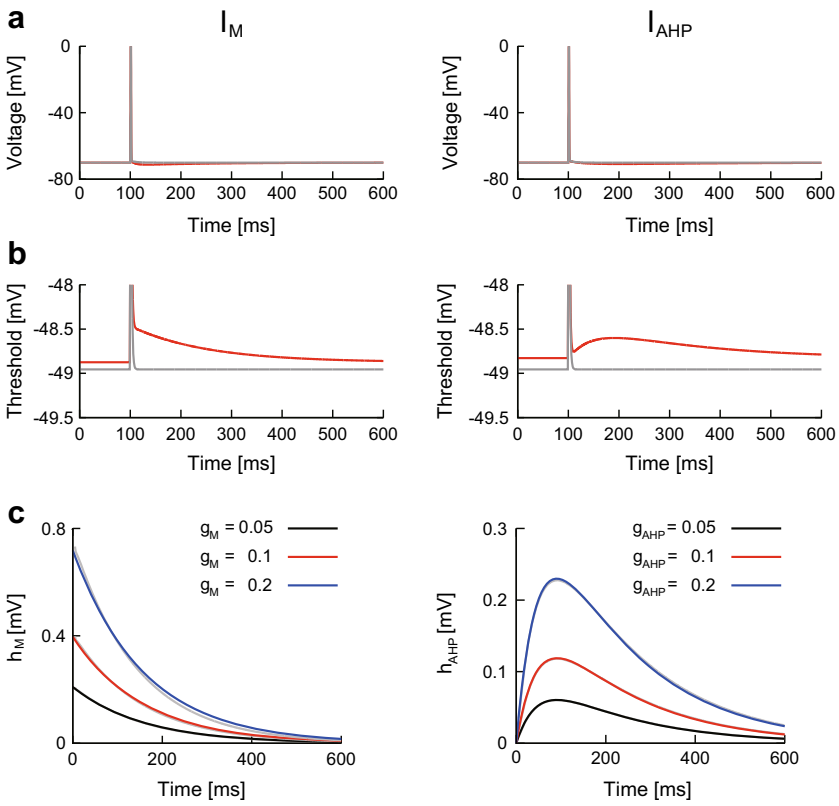

Fig. 4 Effects of slow K^+ currents on the spike threshold. **a**, **b**: The voltage (**a**) and the spike threshold (**b**) of the neuron with I_{M} (left, red) and of the neuron with I_{AHP} (right, *red*) were compared to the corresponding values for the model neuron with no adaptation (*gray*). **c**: The threshold variations in the detailed model neurons, h_{M} (left, *gray*) and h_{AHP} (right, *gray*), were compared to the approximate formulae (Eqs. 21, 22) (*black*, *red*, and *blue*). The maximal conductances (g_{M}, g_{AHP}) were tested at three levels. Other parameter values were given in Table 1

3.4 Reduction of the detailed conductance-based neuron model

The conductance-based neuron model can be reduced to an adaptive threshold model (Section 2.4),

$$\frac{du}{dt} = -\frac{u}{\tau_m} + \frac{I_{\mathrm{ex}}}{C_m}, \quad \text{If } u(t) > \theta_u(t) \rightarrow \text{Emit a spike at time } t, \tag{23}$$

where τ_m is the membrane time constant and θ_u is the spike threshold for u (effective spike threshold) written as

$$\theta_u(t) = \theta_u^{\infty} + \sum\nolimits_k H_u(t - t_k), \tag{24}$$

t_k is the k-th spike time, and $H_u(t)$ is the effective threshold kernel that describes how the effective spike threshold changes after a spike.

We investigated the effect of the slow K^+ current parameters on the effective threshold kernel. The threshold kernel $H_u(t)$ of the neuron with I_{M} can be described by the sum of two exponentials,

$$H_u(t) \approx \alpha_0 e^{-t/\tau_m} + \alpha_{\mathrm{M}} e^{-t/\tau_p\left(\bar{v}\right)}. \tag{25}$$

The threshold kernel is always a monotonically decreasing function in the neuron with I_{M} (Fig. 5a). We can derive a formula that clarifies the relationship between the slow weight α_{M} and I_{M} parameters (Appendix C),

$$\alpha_{\mathrm{M}} \propto g_{\mathrm{M}}\left(\bar{v} - E_K\right)\delta p / \tau_{\max}, \tag{26}$$

where δp is the changes in the p-gate variable during a spike. As predicted by Eq. (26), the slow weight α_{M} increases as g_{M} increases, and decreases as $\tau_{\max}$ increases (Fig. 6a). Numerical results indicate that I_{M} parameters does not affect on the fast weight α_0 significantly (Fig. 6a).

The threshold kernel $H_u(t)$ of the neuron with I_{AHP} is described by the sum of three exponentials,

$$H_u(t) \approx \alpha_0 e^{-t/\tau_m} + \alpha_{\mathrm{AHP}}\left(e^{-t/\tau_{\mathrm{Ca}}} - e^{-t/\tilde{\tau}_s}\right). \tag{27}$$

Interestingly, the threshold kernel can be a non-monotonic function in the neuron with I_{AHP}, and a hump was observed in $H_u(t)$ (Fig. 5b). We can also derive a formula that clarifies the relation between the slow weight α_{AHP} and I_{AHP} parameters (Appendix C),

$$\alpha_{\mathrm{AHP}} \propto g_{\mathrm{AHP}}\left(\bar{v} - E_K\right)\delta \mathrm{Ca}\,\frac{\tau_{\mathrm{Ca}}\tilde{\tau}_s}{\tau_{\mathrm{Ca}} - \tilde{\tau}_s}, \tag{28}$$

where δCa is the changes in Ca^{2+} concentration during a spike. As predicted by Eq. (28), the slow weight α_{AHP} increases as g_{AHP} increases, and decreases as β_s or τ_{Ca} increases (Fig. 6b). Numerical results indicate that I_{AHP} parameters does not affect on the fast weight α_0 significantly (Fig. 6b).

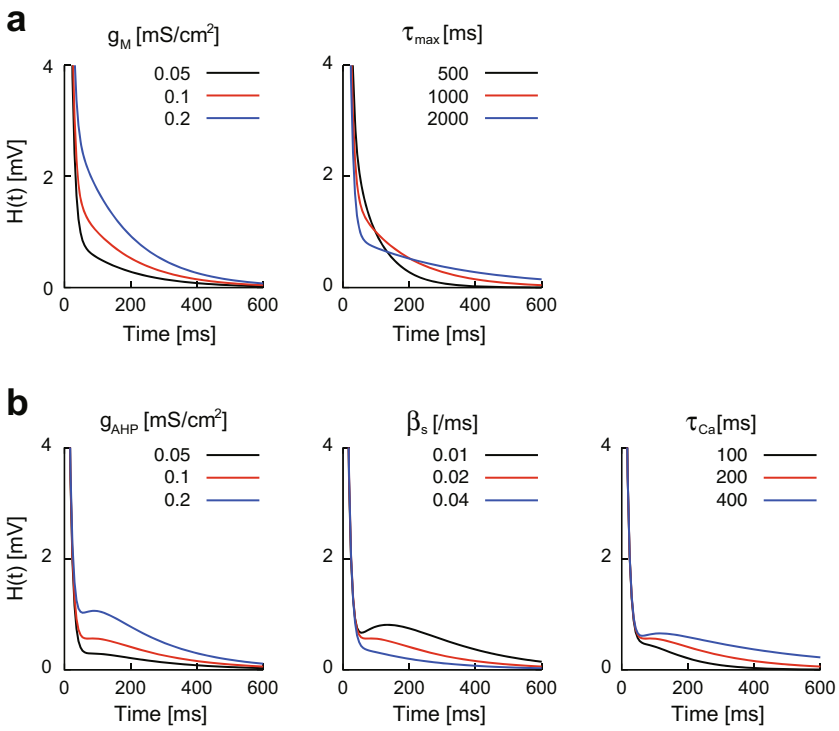

Fig. 5 Effective threshold kernel $H(t)$ in the detailed neuron model. The effective threshold kernel was calculated from the detailed neuron model with I_{M} (**a**) and from the neuron with I_{AHP} (**b**). Each parameter (**a**: g_{M} and $\tau_{\max}$; **b**: g_{AHP}, β_s, and τ_{Ca}) was tested at three levels. Other parameter values were given in Table 1

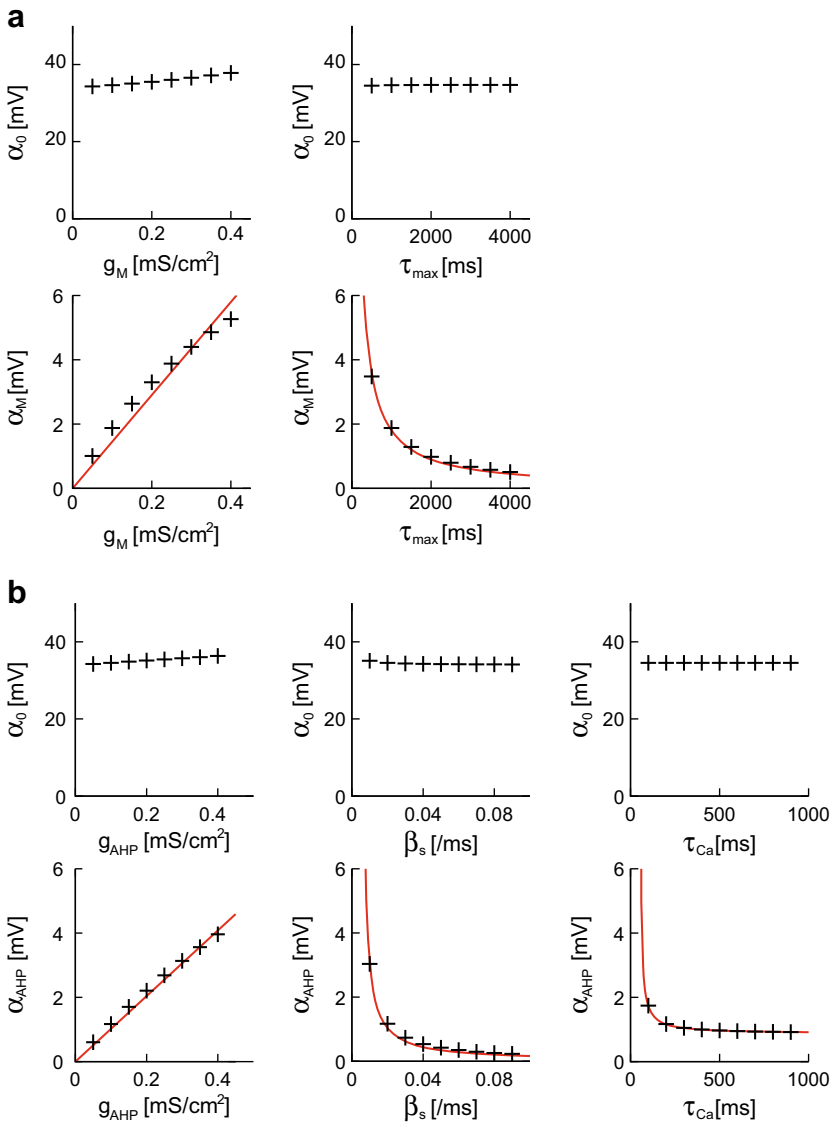

Fig. 6 Influence of the slow K^+ parameters on the threshold kernel. **a**: Scatter plot of the I_M parameters (g_M, τ_{max}) in the detailed neuron model vs. the weights of the threshold kernel (α_0, α_M) in the reduced model. **b**: Scatter plot of the I_{AHP} parameters (g_{AHP}, β_s, and τ_{Ca}) in the detailed neuron model vs. the weights (α_0, α_{AHP}) in the reduced model. Fitted results from the detailed model (crosses) were compared with the approximate formula (Eq. 26, 28, *red lines*)

3.5 Validation of the reduced model

We evaluated the reduced model (Eqs. (23), (24), (25), and (27)) by predicting spike trains of the detailed neuron model using the reduced model. Two sets of input–output data $\{I(t), V(t)\}$ (training data and test data) were generated by injecting fluctuating currents (Eq. (8)) to the detailed neuron model for 50 [s]. The reduced model parameters $\left\{C_m, \theta_u^\infty, \alpha_0, \tau_m; \alpha_M, \ \tau_p(v); \alpha_{AHP}, \tau_{Ca}, \tilde{\tau}_s\right\}$ were tuned from an input–output data set (training data). The membrane capacitance and I_{AHP} time constants were adapted from the detailed model, i.e., $C_m = 1.0$ [nF/cm^2], $\tau_{Ca} = 200$ [ms], and $\tilde{\tau}_s = 50$[ms], and the membrane time constant was inferred from the leak conductance $\tau_m = 10$ [ms]. The p-gate time constant was approximated by its average, $\tau_p(v) \approx \tau_p(\bar{v})$, where $\bar{v}$ is the average voltage. The threshold parameters $\{\theta_u^\infty, \alpha_0, \alpha_M\}$ for the neuron with I_M and $\{\theta_u^\infty, \alpha_0, \alpha_{AHP}\}$ for the neuron with I_{AHP} were determined by maximizing the coincidence factor Γ (Section 2.5) using the simplex downhill method (Kobayashi et al. 2009). Then, the predictive performance was evaluated by calculating the coincidence factor from the other data set (test data) that was not used for parameter optimization. We found that the reduced model can accurately predict spike trains of the detailed model (Fig. 7). The predictive performance Γ for the input currents was 0.854 ± 0.01 (means $\pm$ standard errors, unless stated otherwise) for the neuron with I_M, and 0.903 ± 0.01 for the neuron with I_{AHP}, and the results are summarized in Table 2. The threshold parameters were $\theta_u^\infty = 30.7$ [mV], $\alpha_0 = 35.5$ [mV], and $\alpha_M = 4.1$ [mV] for the neuron with I_M and $\theta_u^\infty = 30.7$ [mV], $\alpha_0 = 32.9$ [mV], and $\alpha_{AHP} = 2.1$ [mV] for the neuron with I_{AHP}.

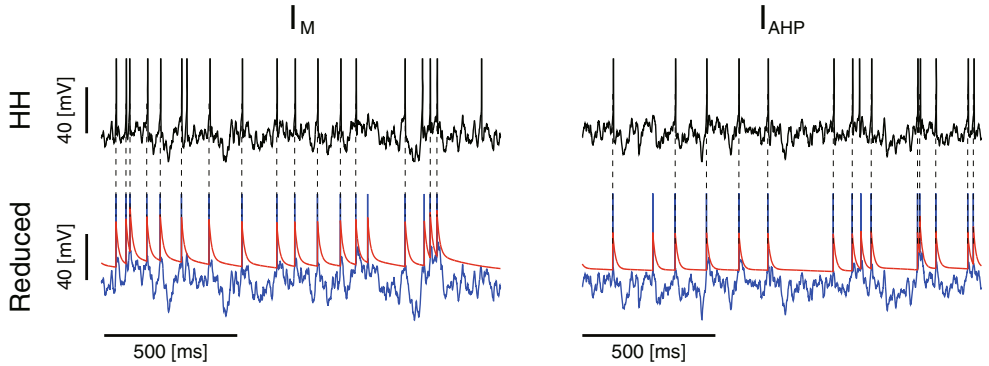

Fig. 7 The reduced model can predict the spike timing of the detailed model. Top: Voltage traces of the detailed neuron model with I_M (*left*) and that with I_{AHP} (*right*). Bottom: Spike timing prediction by the reduced model. The coincidence spikes within 4 [ms] were connected by *dotted lines* and the predictive score Γ were 0.85 (*left*) and 0.87 (*right*). *Blue* and *red* represent the potential u and threshold θ_u, respectively. The parameters were $g_M = 0.2$ [mS/cm^2], $\mu = 2.45$ [V/s], and $\sigma = 2.45$ [mV/$\sqrt{\text{ms}}$] (*left*) and $g_{AHP} = 0.2$ [mS/cm^2], $\mu = 2.4$ [V/s], and $\sigma = 2.4$ [mV/$\sqrt{\text{ms}}$] (*right*)

3.6 Coding property of the reduced model

We analyzed the impact of slow K^+ currents on the coding property of a neuron using the reduced model. Here, we focused on the effect of the input noise on firing irregularity. First, we considered that the reduced model neuron (Eqs. (23) and (24)) is stimulated by a constant current, $I_{ex}(t) = I_0$. An asymptotic periodic solution with period T is written as

$$u(t) = I_0\tau_m \,, \theta_u(t) = \theta_u^\infty + \eta_T^\infty\left(t - t_f\right). \tag{29}$$

where t_f is the most recent spike time, and $\eta_T^\infty(t)$ describes the threshold variation between the spikes; $\eta_T^\infty(t)$ for the neuron with I_M is

$$\eta_T^\infty(t) = \alpha_0 \frac{e^{-t/\tau_m}}{1-e^{-T/\tau_m}} + \alpha_M \frac{e^{-t/\tau_p\left(\bar{v}\right)}}{1-e^{-T/\tau_p\left(\bar{v}\right)}}\,, \tag{30}$$

and $\eta_T^\infty(t)$ for the neuron with I_{AHP} is

$$\eta_T^\infty(t) = \alpha_0 \frac{e^{-t/\tau_m}}{1-e^{-T/\tau_m}} + \alpha_{AHP}\left(\frac{e^{-t/\tau_{Ca}}}{1-e^{-T/\tau_{Ca}}} - \frac{e^{-t/\tilde{\tau}_s}}{1-e^{-T/\tilde{\tau}_s}}\right). \tag{31}$$

The spike condition at the next spike, $t = t_f + T$, leads to

$$\theta_u\left(t_f + T\right) = \theta_u^\infty + \eta_T^\infty(T) = I_0\tau_m. \tag{32}$$

We can analytically evaluate the firing rate $f = T^{-1}$ by solving Eq. (32), and the analytical results are in agreement with *f-I* curves calculated from simulated spike trains (Fig. 8a). The *f-I* curve of the neuron without adaptation ($g_M = g_{AHP} = 0$) can be explicitly written as

$$f = \tau_m^{-1}\log^{-1}\left(1 + \frac{\alpha_0}{I_0\tau_m - \theta_u^\infty}\right), \tag{33}$$

which is similar to the *f-I* curve of the LIF neuron. Note that the response of the reduced model with I_M to the constant current (Eqs. (29) and (30)) is equivalent to the response of the time-dependent threshold model (Tuckwell 1978; Lindner and Longtin 2005; Tamborrino 2016).

Next, we examined the effect of the input noise on spiking irregularity. We have not been able to derive a full analytical result for this effect; however, it is possible to predict the effect of the input noise with the following argument. Let us consider a situation in which a neuron is stimulated by the constant current before the N-th spike ($N \gg 1$) and stimulated by the constant current with small noise after the N-th spike. We can evaluate how the input noise changes the timing of the

Table 2 Accuracy of spike prediction using the reduced model

Current	Firing rate [Hz]	Γ (with I_M)	Γ (with I_{AHP})
M	5	0.823	0.884
M	10	0.805	0.916
M	20	0.854	0.907
H	5	0.886	0.919
H	10	0.894	0.901
H	20	0.862	0.892

The performance of spike prediction for the detailed neuron models using the reduced model is summarized. Each neuron was injected with six fluctuating input currents. Current "M" denotes moderately noisy input ($\sigma = \mu$) and current "H" denotes highly noisy input ($\sigma = 2\mu$)

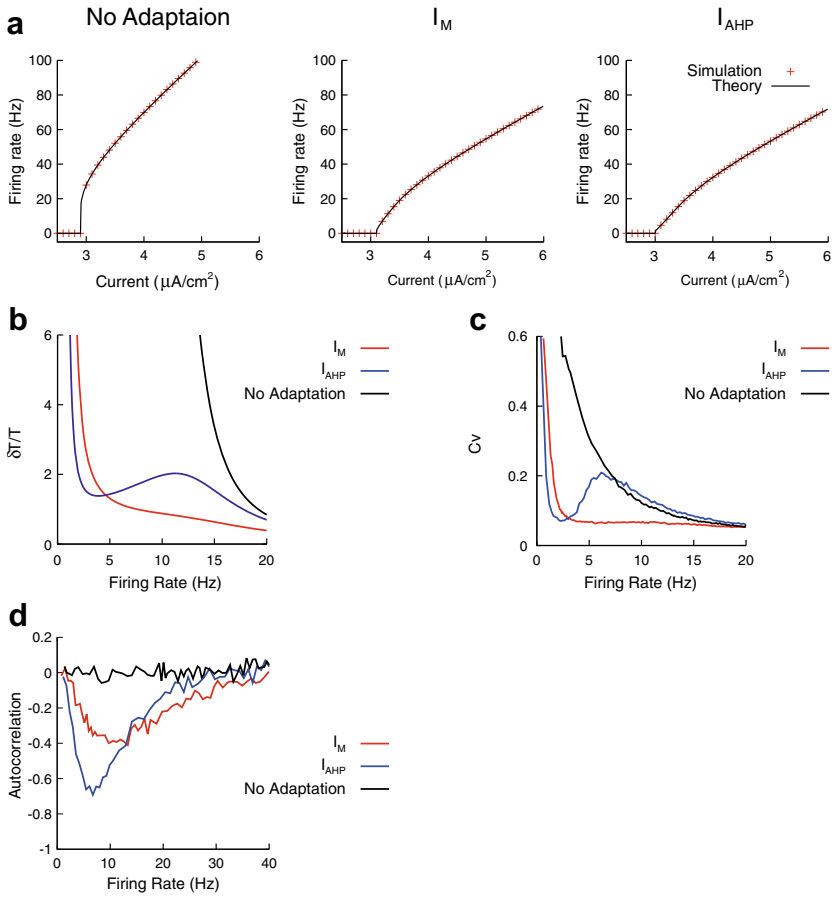

Fig. 8 Effect of the input noise on the coding property of a neuron. **a**: *f-I* curve of the reduced neurons. Analytical result (Eq. 34, *black line*) was compared with the simulation result (*red*). The reduced model parameters were $\theta_u^\infty = 29$ [mV], $\alpha_0 = 35$ [mV], and $\tau_m = 10$ [ms] for the neuron without adaptation, $\theta_u^\infty = 31$ [mV], $\alpha_0 = 36$ [mV], $\alpha_M = 1.6$ [mV], $\tau_m = 10$ [ms], and $\tau_p(\bar{v}) = 150$ [ms] for the neuron with I_M and $\theta_u^\infty = 30$ [mV], $\alpha_0 = 34$ [mV], $\alpha_{AHP} = 2.6$ [mV], $\tau_m = 10$ [ms], $\tau_{Ca} = 200$ [ms], and $\tau_s = 100$ [ms] for the neuron with I_{AHP}. **b**: Effect of the slow K^+ currents on spiking irregularity (Analytical result, Eq. 35 with $\delta u = 1$). **c**: Effect of the slow K^+ currents on Cv of ISIs (Simulated result). Fluctuate currents (Eq. 8) were injected to the detailed model neurons. The input mean μ was changed to control the firing rate, whereas the input variance σ was fixed: $\sigma = 0.04$ [mV/$\sqrt{}$ms]. The neuron parameters were $g_M = 0.1$ [mS/cm^2] for the neuron with I_M and $g_{AHP} = 0.1$ [mS/cm^2], $\beta_s = 0.01$ [/ms] for the neuron with I_{AHP}, and other parameter were given in Table 1. **d**: Effect of the slow K^+ currents on autocorrelation. The autocorrelation was calculated from spike trains generated from the reduced model. The parameters were same as **a**

subsequent spike. At the $(N+1)$-th spike time, the threshold should cross the potential

$$\theta_u(t_N + T + \delta T) = I_0\tau_m + \delta u, \tag{34}$$

where t_N is the N-th spike time, δT and δu are perturbations due to the small noise. By Taylor-expanding θ_u assuming that δT is small, we obtain

$$\delta T \simeq {}^{\delta u}\Big/ \frac{d\eta_T^\infty}{dt}(T). \tag{35}$$

Equation (35) indicates that slow K^+ currents improve the robustness against noise in a different manner (Fig. 8b), i.e., I_M suppresses the spike interval dispersion $\delta T/T$ for a broad firing range, whereas I_{AHP} suppress the dispersion only at a low firing range (~3 [Hz]). The dispersion $\delta T/T$ is not identical to the coefficient of variation (Cv) of interspike intervals (ISIs), however it has a close relation to Cv. We found that this differential effect was also observed in Cv of the detailed model with slow K^+ currents (Fig. 8c). Finally, we examined how the slow K^+ currents modulate autocorrelation of a spike train that was defined as $\rho_1 = \langle ISI_i ISI_{i+1} - \langle ISI_i \rangle^2 \rangle / \langle ISI_i^2 - \langle ISI_i \rangle^2 \rangle$, where ISI_i is the i-th ISI and $\langle \dots \rangle$ is the averaging over index i. The autocorrelation quantifies how often a long ISI is followed by a short ISI and vice versa. The neuron model with the slow K^+ currents can reproduce the negative ISI correlation, which was commonly observed in sensory periphery and cortical neurons (Farkhooi et al. 2009). As shown in Fig. 8d, the effect of I_{AHP} on the autocorrelation is stronger than that of I_M in the low firing rate regime (<15 [Hz]), whereas the effect of I_{AHP} is similar to that of I_M in the high firing rate regime (>15 [Hz]). A previous work

(Chacron et al. 2001) showed that the negative ISI correlation can improve the capacity for encoding time-varying stimulus. Our result implies that the slow K^+ currents improve the encoding of time-varying stimulus in a different way.

4 Discussion

We have shown that the detailed conductance-based neuron model with slow K^+ currents (I_M and I_{AHP}) can be reduced to an adaptive threshold model. The reduced model is written as

$$\begin{aligned} &\frac{du}{dt} = -\frac{u}{\tau_m} + \frac{I_{ex}}{C_m}, \quad \text{If } u(t) > \theta_u(t) \rightarrow \text{Emits a spike at time } t, \\ &\theta_u(t) = \theta_u^{\infty} + \sum\nolimits_k H_u(t - t_k), \\ &H_u(t) = \alpha_0 e^{-t/\tau_m} + \alpha_M e^{-t/\tau_p}\left(\overline{v}\right) + \alpha_{AHP}\left(e^{-t/\tau_{Ca}} - e^{-t/\tilde{\tau}_s}\right), \end{aligned} \tag{36}$$

where θ_u is the spike threshold for u, and $H_u(t)$ is the threshold kernel. We have also derived formulae that describe the relationship between slow K^+ current parameters and reduced model parameters (Eqs. (26) and (28)), which provide a physiological interpretation of the reduced model. The reduced model can accurately predict spike trains of the detailed model (Fig. 7). Our analysis of the reduced model revealed that slow K^+ currents have differential effects on noise tolerance of a neuron, i.e., I_M suppresses firing irregularity regardless of the firing rate, whereas I_{AHP} suppresses firing irregularity only at a low firing range (Fig. 8b, c). The slow K^+ currents induce negative interspike interval correlations, and the effect of I_{AHP} is stronger than that of I_M in the low firing regime (Fig. 8d).

4.1 Mapping a detailed conductance-based neuron model to a simplified model

As noted in the Introduction, one approach of obtaining a reduced model is to develop a mathematical framework from detailed neuron models to simplified models. This approach has clarified the relationship between these models. For example, the FitzHugh–Nagumo model was derived from the Hodgkin–Huxley model by assuming that Na^+ activation (m) is instantaneous and that Na^+ inactivation (h) and K^+ activation (n) change with a similar time constant (Abbott and Kepler 1990; Rinzel and Ermentrout 1998). A generalized integrate-and-fire model can also be derived from the Hodgkin–Huxley model by linearization (Destexhe 1997; Koch 1999; Richardson et al. 2003).

In this study, we have extended the linearization approach by including the spike history effect, which is essential for describing the effect of slow K^+ currents on spike generation. The linearized model is a simple linear equation with the effective threshold $\theta_u(t)$ (Eq. (36)) that incorporates the effect of ionic currents and spike threshold variation on neuronal excitability. We have shown that the effective threshold obtained from the detailed model with slow K^+ current can be approximated by a modified multi-timescale adaptive threshold (MAT) model (Kobayashi et al. 2009).

4.2 Reduced neuron model

Spike-frequency adaptation can be described by simplified models with adaptation, which is modeled by adaptive current (Liu and Wang 2001; Brette and Gerstner 2005; Izhikevich 2007) or adaptive threshold (Chacron et al. 2000, 2007; Liu and Wang 2001; Jolivet et al. 2004, 2006, 2008). The adaptive threshold models can reproduce the interspike interval statistics (Chacron et al. 2000), *f-I* curve (Rauch et al. 2003; Kobayashi 2009), and spike timings (Jolivet et al. 2006, 2008) of a neuron recorded in experiments. On the other hand, the adaptive threshold model was criticized because, unlike the adaptive current model, it cannot reproduce the lateral shift of *f-I* curves observed in experiments (Benda et al. 2010). Note that the derived MAT model (Eq. (36)) incorporates both effects, i.e., the effect of the adaptive current and threshold. This fact can explain the success of the MAT model in accurately predicting spike times (Kobayashi et al. 2009; Yamauchi et al. 2011).

The derived model has two advantages. First, the model is essentially linear; the linearity makes mathematical analysis tractable. Indeed, it is possible to examine the effect of noise on firing irregularity, which can predict a qualitative behavior of the detailed model (Fig. 8). In addition, the linearity enables us to efficiently simulate a network of neurons by the exact sub-threshold integration (Morrison et al. 2007; Yamauchi et al. 2011). Second, the reduced model offers a clear relationship between the slow K^+ parameters and reduced model parameters (Eqs. (26) and (28)). This relationship is important because it enables us to analyze the effect of slow K^+ currents using the reduced model.

4.3 Spike threshold variation in experiments

Conventionally, it was considered that a neuron has a fixed voltage threshold for generating an action potential. However, experimental studies *in vivo* have suggested that the spike threshold is not constant but is highly variable (Azouz and Gray 2000; Henze and Buzsaki 2001; Chacron et al. 2007). Studies in the rodent hippocampus (Henze and Buzsaki 2001) and fish (Chacron et al. 2007) have demonstrated that the spike threshold increases after each action potential, which is referred to as "*threshold fatigue.*" We found that the spike threshold of the detailed neuron model jumps

and decays exponentially after each spike with a time constant of ~100 [ms] (Fig. 4), suggesting that slow K^+ currents may be the possible cellular mechanism underlying *threshold fatigue*. Other biophysical mechanisms, particularly Na^+ currents, may underlie the threshold variability. The spike threshold also varies with the voltage derivative preceding a spike (Azouz and Gray 2000). Interestingly, it was shown that Na^+ inactivation modulates the spike threshold, which varies with the membrane voltage with a small time constant ($\tau_h(v) \approx 2 \sim 10$ [ms]) (Platkiewicz and Brette 2010; Fontaine et al. 2014) and Na^+ inactivation can explain the voltage-dependence of the spike threshold observed in experiments (Platkiewicz and Brette 2011). The modulation of the spike threshold differs depending on its factor, in other words, the threshold modulation by slow K^+ currents is slow and accumulative, whereas that by Na^+ inactivation is rapid.

The instantaneous spike threshold of layer-5 pyramidal neurons has been estimated from the membrane potential recorded *in vitro* (Badel et al. 2008). The results suggest that the threshold modulation after a spike is described by the sum of two exponentials, $\theta_V(\mathrm{t}) \approx \theta_V^\infty + A_1 e^{-(t-t_f)/\tau_1} + A_2 e^{-(t-t_f)/\tau_2}$, where $\theta_V(\mathrm{t})$ is the spike threshold and t_f is the most recent spike time. The fast components were $A_1 \approx 10$ [mV] and $\tau_1 \approx 20$ [ms], whereas the slow components were $A_2 \approx 1$ [mV] and $\tau_2 \approx 100$ [ms]. The detailed model used here reproduces the slow component in the threshold modulation; however, it does not reproduce the fast component. This is presumably due to the difference in Na^+ current kinetics that describes the shape of an action potential. Indeed, it was reported that the spike waveform recorded from experiments is much shaper than that of Hodgkin–Huxley models (Badel et al. 2008).

4.4 Functional implications of the slow K^+ currents

It is well known that slow K^+ currents induce the spike-frequency adaptation, which acts as a spike-triggered self-inhibition (Fig. 2; Benda and Herz 2003; Prescott and Sejnowski 2008). Several studies have proposed functional consequences of spike-frequency adaptation. For instance, the adaptation generates the "forward masking" effect, which suppresses the neuronal response under a prolonged stimulus (Liu and Wang 2001), improve signal transmission for low frequency stimulus (Chacron et al. 2007), and contributes to sparse and reliable coding (Farkhooi et al. 2013). Here, we have derived a simplified model that can reproduce the differential effects of slow K^+ currents. The reduced model can accurately predict spike trains of the detailed neuron model (Fig. 7) and reproduce the *f-I* curve and spike train power spectrum (Data not shown).

Previous studies have suggested that slow K^+ currents have differential effects on the coding property of a single neuron. For instance, I_M facilitates spike-timing coding because it improves the robustness of spike pattern against the input noise. In contrast, I_{AHP} enhances spike-rate coding, because it regularizes the spike train elicited by slow inputs (Prescott and Sejnowski 2008). It has also been suggested that I_M increases, whereas I_{AHP} decreases, the response to low-frequency input signals (Deemyad et al. 2012). Our analysis revealed a new differential effect underlying slow K^+ currents (Fig. 8b, c), i.e., I_M suppresses firing irregularity regardless of the firing rate, whereas I_{AHP} suppresses the irregularity only at a low firing range (~3 [Hz]). This result suggests that neurons with I_{AHP} can contribute to the generation of rhythmical activity at a low firing rate. We hope that the reduced model will be useful for analyzing how the slow K^+ currents impact on the coding properties of single neurons and neural populations.

Acknowledgments This study was supported by JSPS KAKENHI Grant Number 25115728, 25870915 to RK, and 24500372, 15H05877 to KK. We thank Shigeru Shinomoto and Romain Brette for stimulating discussions, and two anonymous reviewers for helpful comments.

Compliance with ethical standards

Conflict of interest The authors declare that they have no conflict of interest.

Appendix A: Approximate formulae for spike triggered ionic currents: η_M, η_{AHP}

We derive approximate formulae for the spike-triggered current induced by slow K^+ currents. For simplicity, we consider a situation in which the neuron generates a spike at $t = 0$ [ms], and the input current is constant.

A.1. M current We replace a spike with a rectangular pulse with a peak voltage v_1 and a width w_{sp} (Destexhe 1997). The differential equation for the p (Table 1) can be simplified to

$$\frac{d\tilde{p}}{dt} = \begin{cases} -\dfrac{\tilde{p} - p_\infty(v_1)}{\tau_p(v_1)} & (\mathrm{Spike} : 0 < t < w_{\mathrm{sp}}) \\ -\dfrac{\tilde{p} - p_\infty(\bar{v})}{\tau_p(\bar{v})} & (\mathrm{Otherwise} : w_{\mathrm{sp}} < t), \end{cases} \tag{37}$$

where $\tilde{p}$ is an approximation of p and $\bar{v}$ is an equilibrium voltage after a spike. The solution of Eq. (37) is

$$\tilde{p}(t) = \begin{cases} p_\infty(v_1) + \left(\tilde{p}(0) - p_\infty(v_1)\right) e^{-t/\tau_p(v_1)} & (0 < t < w_{\mathrm{sp}}) \\ p_\infty(\bar{v}) + \left(\tilde{p}(w_{\mathrm{sp}}) - p_\infty(\bar{v})\right) e^{-(t-w_{\mathrm{sp}})/\tau_p(\bar{v})} & (w_{\mathrm{sp}} < t). \end{cases} \tag{38}$$

Based on Eq. (38), the equilibrium conductance is given by $\overline{g}_{\mathrm{M}} = g_{\mathrm{M}}\, p_\infty(\overline{v})$. The spike-triggered current after the spike is written as

$$\eta_{\mathrm{M}}(t) \approx g_{\mathrm{M}}\left(\tilde{p}(t) - p_\infty\left(\overline{v}\right)\right)\,(v(t) - E_K), \tag{39}$$

where $v(t)$ is the membrane voltage. By substituting Eq. (38) into (39), we obtain

$$\eta_{\mathrm{M}}(t) \approx a_{\mathrm{M}} e^{-t/\tau_p\left(\overline{v}\right)}, \tag{40}$$

where $a_{\mathrm{M}} = g_{\mathrm{M}}(\overline{v} - E_K)\left(\tilde{p}\left(w_{\mathrm{sp}}\right) - p_\infty(\overline{v})\right)\, e^{w_{\mathrm{sp}}/\tau_p(\overline{v})}$. A more accurate formula can be obtained by incorporating the spike waveform. Voltage after a spike can be approximated by an exponential function $v(t) \approx \delta v e^{-t/\tau_m} + \overline{v}$,

$$\eta_{\mathrm{M}}(t) \approx a_M^1 e^{-t/\tau_m} + a_M^2 e^{-t/\tau_p\left(\overline{v}\right)}, \tag{41}$$

where τ_m is the membrane time constant and

$$a_{\mathrm{M}}^1 = g_{\mathrm{M}}\delta v\left(\tilde{p}\left(w_{\mathrm{sp}}\right) - \tilde{p}_\infty(\overline{v})\right)e^{w_{\mathrm{sp}}/\tau_p(\overline{v})},\ a_{\mathrm{M}}^2 = a_{\mathrm{M}}.$$

We assumed that the membrane time constant is much smaller than the time constants of p-gate: $\tau_m \ll \tau_p(\overline{v})$. Equation (41) is more accurate than Eq. (40) in the short period ($t < 30$ [ms]) after a spike. In this study, we adopted the simpler formula (40) for simplicity.

A.2. AHP current Because the Ca^{2+} current is fast (Fig. 3a) compared to the time constant of Ca^{2+} outflux (: $\tau_{\mathrm{Ca}} \approx 200$ [ms]), we can approximate the calcium current with a short pulse, $I_{\mathrm{Ca}} \approx q_{\mathrm{Ca}}\delta(t)$. The Ca^{2+} concentration after a spike at time t is

$$\left[\mathrm{Ca}^{2+}\right] \approx \delta\mathrm{Ca}\, e^{-t/\tau_{\mathrm{Ca}}} + \left[\mathrm{Ca}^{2+}\right]_\infty, \tag{42}$$

where $\delta\mathrm{Ca} = -5.0 \times 10^4 \times q_{\mathrm{Ca}}/\mathrm{F}$ represents Ca^{2+} influx during a spike. Because the Ca^{2+} concentration is very small, s-gate time constant can be approximated as $\tau_s = (\alpha_s + \beta_s)^{-1} \approx \beta_s^{-1} =: \tilde{\tau}_s$. Hence, we obtain

$$\frac{d\tilde{s}}{dt} = -\tilde{s}/\tilde{\tau}_s + 0.01\left[\mathrm{Ca}^{2+}\right](t), \tag{43}$$

where $\tilde{s}$ is an approximation of the s-gate variable s. By substituting Eq. (42) into (43), we can solve the differential equation analytically as,

$$\tilde{s}(t) = a_s\left(e^{-t/\tau_{\mathrm{Ca}}} - e^{-t/\tilde{\tau}_s}\right) + s_\infty, \tag{44}$$

where $a_s = \frac{0.01\tau_{\mathrm{Ca}}\tilde{\tau}_s}{\tau_{\mathrm{Ca}} - \tilde{\tau}_s}\delta\mathrm{Ca}$, $s_\infty = 0.01\left[\mathrm{Ca}^{2+}\right]_\infty\tilde{\tau}_s$. As with the case of I_{M}, the equilibrium conductance is given by $\overline{g}_{\mathrm{AHP}} = g_{\mathrm{AHP}}s_\infty$. The spike-triggered current is

$$\eta_{\mathrm{AHP}}(t) \approx g_{\mathrm{AHP}}\left(\tilde{s}(t) - s_\infty\right)(v(t) - E_{\mathrm{K}}), \tag{45}$$

By substituting Eq. (44) into (45) and replacing the voltage with its equilibrium value $\overline{v}$, we obtain

$$\eta_{\mathrm{AHP}}(t) \approx a_{\mathrm{AHP}}\left(e^{-t/\tau_{\mathrm{Ca}}} - e^{-t/\tilde{\tau}_s}\right), \tag{46}$$

where $a_{\mathrm{AHP}} = g_{\mathrm{AHP}}(\overline{v} - E_{\mathrm{K}})a_s$.

Appendix B: Approximate formula for spike threshold: $h_{\mathrm{M}}(t)$, $h_{\mathrm{AHP}}(t)$

We derive an approximate formula that describes how the slow K^+ currents modulates spike threshold. Close to spike threshold, the membrane voltage of a neuron can be described by the exponential integrate and fire model (Fourcaud-Trocmé et al. 2003; Platkiewicz and Brette 2010),

$$C_m\frac{dV}{dt} = F(V) = -g_{\mathrm{tot}}(V - E_{\mathrm{tot}}) + g_{\mathrm{tot}}\Delta_T e^{(V-V_T)/\Delta_T} - I_{\mathrm{adp}}(t), \tag{47}$$

where $I_{\mathrm{adp}}(t) = \sum_{k:\ t_k < t}\eta_{\mathrm{ion}}(t - t_k)$ is the spike-triggered current induced by the slow K^+ currents. The spike threshold θ_V defined by a critical voltage above which the neuron emits a spike, $F(\theta_V) = 0$, is given by

$$\theta_V \approx V_T + \Delta_T\log\left(\frac{V_T - E_{\mathrm{tot}} + RI_{\mathrm{adp}}}{\Delta_T}\right), \tag{48}$$

where $R = g_{\mathrm{tot}}^{-1}$ is the membrane resistance. If RI_{adp} is small compared to $V_T - E_{\mathrm{tot}}$, Eq. (48) can be simplified further,

$$\theta_V \approx V_T + \Delta_T\log\left(\frac{V_T - E_{\mathrm{tot}}}{\Delta_T}\right) + \frac{R\Delta_T}{V_T - E_{\mathrm{tot}}}I_{\mathrm{adp}}. \tag{49}$$

The variation of spike threshold by an ionic current can be given by

$$h_{\mathrm{ion}} \approx \frac{R\Delta_T}{V_T - E_{\mathrm{tot}}}\eta_{\mathrm{ion}}. \tag{50}$$

We can see from Eq. (50) that the threshold variation h_{ion} is approximately proportional to the spike-triggered current η_{ion}.

Appendix C: Relating the reduced model to the MAT model

By substituting Eqs. (19) − (22) into (17), the effective spike threshold modulated by a spike can be written as

$$\begin{aligned} H(t) = &-\delta V e^{-\left(t - w_{\mathrm{sp}}\right)/\tau_{\mathrm{m}}} + \frac{a_{\mathrm{M}}}{C_m}f_{De}\left(\tau_p\left(\overline{v}\right), \tau_m\right) \\ &+ \frac{a_{\mathrm{AHP}}}{C_m}\left\{f_{De}(\tau_{\mathrm{Ca}}, \tau_m) - f_{De}\left(\tilde{\tau}_s, \tau_m\right)\right\} \\ &+ b_{\mathrm{M}}e^{-t/\tau_p\left(\overline{v}\right)} + b_{\mathrm{AHP}}\left(e^{-t/\tau_{\mathrm{Ca}}} - e^{-t/\tilde{\tau}_s}\right), \end{aligned} \tag{51}$$

where $f_{De}(\tau_1, \tau_2) := \left(e^{-t/\tau_1} - e^{-t/\tau_2}\right)/\left(\tau_2^{-1} - \tau_1^{-1}\right)$ and the time constants are given in Eqs. (19) and (20). If we assume that the

membrane time constant is much smaller than the slow K^+ time constants: $\tau_m \ll \tau_p(\bar{v})$, τ_{Ca}, $\tilde{\tau}_s$, the formula can be simplified further,

$$H(t) \approx \alpha_0 e^{-t/\tau_m} + \alpha_{\mathrm{M}} e^{-t/\tau_p\left(\bar{v}\right)} + \alpha_{\mathrm{AHP}}\left(e^{-t/\tau_{\mathrm{Ca}}} - e^{-t/\tilde{\tau}_s}\right), \quad (52)$$

where the weights are $\alpha_0 = -\delta V e^{w_{\mathrm{sp}}/\tau_{\mathrm{m}}} - a_M/g_{\mathrm{tot}}$, $\alpha_{\mathrm{M}} = a_M/g_{\mathrm{tot}} + b_{\mathrm{M}}$, $\alpha_{\mathrm{AHP}} = a_{\mathrm{AHP}}/g_{\mathrm{tot}} + b_{\mathrm{AHP}}$. The slow weights can be related to the slow K^+ parameters by using Eqs. (40), (46), (50),

$$\alpha_{\mathrm{M}} \propto a_{\mathrm{M}} \propto g_{\mathrm{M}}\left(\bar{v} - E_K\right)\delta p, \quad \alpha_{\mathrm{AHP}} \propto a_{\mathrm{AHP}} \propto g_{\mathrm{AHP}}\left(\bar{v} - E_{\mathrm{K}}\right)\delta \mathrm{Ca}\,, \quad (53)$$

where $\delta p := \tilde{p}\left(w_{\mathrm{sp}}\right) - p_\infty(\bar{v})$ and δCa are the changes in p and $[Ca^{2+}]$ during a spike.

References

Abbott, L., & Kepler, T. (1990). Model neurons: from Hodgkin − Huxley to Hopfield. In L. Garrido (Ed.), *Statistical Mechanics of Neural Networks*. Berlin: Springer.

Adams, P. R., Brown, D. A., & Constanti, A. (1982). Pharmacological inhibition of the M-current. *The Journal of Physiology, 332*, 223–262.

Azouz, R., & Gray, C. M. (2000). Dynamic spike threshold reveals a mechanism for synaptic coincidence detection in cortical neurons in vivo. *Proceedings of the National Academy of Sciences of the United States of America, 97*, 8110–8115.

Badel, L., Lefort, S., Brette, R., Petersen, C. C., Gerstner, W., & Richardson, M. J. (2008). Dynamic IV curves are reliable predictors of naturalistic pyramidal-neuron voltage traces. *Journal of Neurophysiology, 99*, 656–666.

Benda, J., & Herz, A. V. M. (2003). A universal model for spike-frequency adaptation. *Neural Computation, 15*, 2523–2564.

Benda, J., Maler, L., & Longtin, A. (2010). Linear versus nonlinear signal transmission in neuron models with adaptation currents or dynamic thresholds. *Journal of Neurophysiology, 104*, 2806–2820.

Brette, R., & Gerstner, W. (2005). Adaptive exponential integrate-and-fire model as an effective description of neuronal activity. *Journal of Neurophysiology, 94*, 3637–3642.

Brown, D. A., & Adams, P. R. (1980). Muscarinic suppression of a novel voltage-sensitive K^+ current in a vertebrate neurone. *Nature, 283*, 673–676.

Brown, D. A., & Griffith, W. H. (1983). Calcium-activated outward current in voltage-clamped hippocampal neurones of the guinea-pig. *The Journal of Physiology, 337*, 287–301.

Chacron, M. J., Longtin, A., St-Hilaire, M., & Maler, L. (2000). Suprathreshold stochastic firing dynamics with memory in P-type electroreceptors. *Physical Review Letters, 85*, 1576–1579.

Chacron, M. J., Longtin, A., & Maler, L. (2001). Negative interspike interval correlations increase the neuronal capacity for encoding time-dependent stimuli. *Journal of Neuroscience, 21*, 5328–5343.

Chacron, M. J., Lindner, B., & Longtin, A. (2007). Threshold fatigue and information transfer. *Journal of Computational Neuroscience, 23*, 301–311.

Deemyad, T., Kroeger, J., & Chacron, M. J. (2012). Sub- and suprathreshold adaptation currents have opposite effects on frequency tuning. *The Journal of Physiology, 590*, 4839–4858.

Destexhe, A. (1997). Conductance-based integrate-and-fire models. *Neural Computation, 9*, 503–514.

Ermentrout, B., & Kopell, N. (1986). Parabolic bursting in an excitable system coupled with a slow oscillation. *SIAM Journal on Applied Mathematics, 46*, 233–253.

Ermentrout, B., Pascal, M., & Gutkin, B. (2001). The effects of spike frequency adaptation and negative feedback on the synchronization of neural oscillators. *Neural Computation, 13*, 1285–1310.

Farkhooi, F., Strube-Bloss, M. F., & Nawrot, M. P. (2009). Serial correlation in neural spike trains: experimental evidence, stochastic modeling, and single neuron variability. *Physical Review E, 79*, 021905.

Farkhooi, F., Froese, A., Muller, E., Menzel, R., & Nawrot, M. P. (2013). Cellular adaptation facilitates sparse and reliable coding in sensory pathways. *PLoS Computational Biology, 9*, e1003251.

Fleidervish, I. A., Friedman, A., & Gutnick, M. J. (1996). Slow inactivation of Na^+ current and slow cumulative spike adaptation in mouse and guinea-pig neocortical neurones in slices. *The Journal of Physiology, 4931*, 83–97.

Fontaine, B., Pena, J. L., & Brette, R. (2014). Spike-Threshold Adaptation Predicted by Membrane Potential Dynamics. *PLoS Computational Biology, 10*, e1003560.

Fourcaud-Trocmé, N., Hansel, D., Van Vreeswijk, C., & Brunel, N. (2003). How spike generation mechanisms determine the neuronal response to fluctuating inputs. *Journal of Neuroscience, 23*, 11628–11640.

Gerstner, W., & Kistler, W. M. (2002). *Spiking neuron models: Single neurons, populations, plasticity*. Cambridge: Cambridge University Press.

Henze, D. A., & Buzsaki, G. (2001). Action potential threshold of hippocampal pyramidal cells in vivo is increased by recent spiking activity. *Neuroscience, 105*, 121–130.

Izhikevich, E. M. (2007). *Dynamical systems in neuroscience: the geometry of excitability and bursting*. Cambridge: MIT Press.

Jolivet, R., Lewis, T. J., & Gerstner, W. (2004). Generalized integrate-and-fire models of neuronal activity approximate spike trains of a detailed model to a high degree of accuracy. *Journal of Neurophysiology, 92*, 959–976.

Jolivet, R., Rauch, A., Lüscher, H.-R., & Gerstner, W. (2006). Predicting spike timing of neocortical pyramidal neu- rons by simple threshold models. *Journal of Computational Neuroscience, 21*, 35–49.

Jolivet, R., Kobayashi, R., Rauch, A., Naud, R., Shinomoto, S., & Gerstner, W. (2008). A benchmark test for a quantitative assessment of simple neuron models. *Journal of Neuroscience Methods, 169*, 417–424.

Kim, K. J., & Rieke, F. (2003). Slow Na^+ inactivation and variance adaptation in salamander retinal ganglion cells. *Journal of Neuroscience, 23*, 1506–1516.

Kistler, W., Gerstner, W., & van Hemmen, J. L. (1997). Reduction of the Hodgkin-Huxley equations to a single-variable threshold model. *Neural Computation, 9*, 1015–1045.

Kobayashi, R. (2009) The influence of firing mechanisms on gain modulation. *Journal of Statistical Mechanics* P01017.

Kobayashi, R., & Shinomoto, S. (2007). State space method for predicting the spike times of a neuron. *Physical Review E, 75*, 011925.

Kobayashi, R., Tsubo, Y., & Shinomoto, S. (2009). Made-to-order spiking neuron model equipped with a multi-timescale adaptive threshold. *Frontiers in Computational Neuroscience, 3*, 9.

Kobayashi, R., Shinomoto, S., & Lansky, P. (2011). Estimation of time-dependent input from neuronal membrane potential. *Neural Computation, 23*, 3070–3093.

Koch, C. (1999). *Biophysics of computation*. Oxford: Oxford University Press.

Lindner, B., & Longtin, A. (2005). Effect of an exponentially decaying threshold on the firing statistics of a stochastic integrate-and-fire neuron. *Journal of Theoretical Biology, 232*, 505–521.

Liu, Y. H., & Wang, X. J. (2001). Spike-frequency adaptation of a generalized leaky integrate-and-fire model neuron. *Journal of Computational Neuroscience, 10*, 25–45.

Madison, D. V., & Nicoll, R. A. (1984). Control of the repetitive discharge of rat CA1 pyramidal neurones in vitro. *The Journal of Physiology, 354*, 319–331.

Mainen, Z. F., & Sejnowski, T. J. (1996). Influence of dendritic structure on firing pattern in model neocortical neurons. *Nature, 382*, 363–366.

Morrison, A., Straube, S., Plesser, H. E., & Diesmann, M. (2007). Exact subthreshold integration with continuous spike times in discrete-time neural network simulations. *Neural Computation, 19*, 47–79.

Platkiewicz, J., & Brette, R. (2010). A threshold equation for action potential initiation. *PLoS Computational Biology, 6*, e1000850.

Platkiewicz, J., & Brette, R. (2011). Impact of fast sodium channel inactivation on spike threshold dynamics and synaptic integration. *PLoS Computational Biology, 7*, e1001129.

Pospischil, M., Toledo-Rodriguez, M., Monier, C., Piwkowska, Z., Bal, T., Fregnac, Y., Markram, H., & Destexhe, A. (2008). Minimal Hodgkin − Huxley type models for different classes of cortical and thalamic neurons. *Biological Cybernetics, 99*, 427–441.

Prescott, S. A., & Sejnowski, T. J. (2008). Spike-rate coding and spike-time coding are affected oppositely by different adaptation mechanisms. *Journal of Neuroscience, 28*, 13649–13661.

Press, W. H., Teukolsky, S. A., Vetterling, W. T., & Flannery, B. P. (2007). *Numerical recipes: The art of scientific computing* (3rd ed.). Cambridge: Cambridge University Press.

Rauch, A., La Camera, G., Lüscher, H.-R., Senn, W., & Fusi, S. (2003). Neocortical pyramidal cells respond as integrate-and-fire neurons to in-vivo-like input currents. *J Neurophysiol, 90*, 1598–1612.

Richardson, M. J., Brunel, N., & Hakim, V. (2003). From subthreshold to firing-rate resonance. *Journal of Neurophysiology, 89*, 2538–2554.

Rinzel, J., Ermentrout, G. B. (1998) In C. Koch, I. Segev (eds.) *Methods in neuronal modeling* 2nd Edition (pp. 251–291). Cambridge: MIT.

Schwindt, P. C., Spain, W. J., & Crill, W. E. (1989). Long-lasting reduction of excitability by a sodium-dependent potassium current in cat neocortical neurons. *Journal of Neurophysiology, 61*, 233–244.

Tamborrino, M. (2016). Approximation of the first passage time density of a Brownian motion to an exponentially decaying threshold by two-piecewise linear threshold. Application to neuronal spiking activity. *Mathematical Biosciences and Engineering, 13*, 613–629.

Tsubo, Y., Kaneko, T., & Shinomoto, S. (2004). Predicting spike timings of current-injected neurons. *Neural Networks, 17*, 165–173.

Tuckwell, H. C. (1978). Recurrent inhibition and afterhyperpolarization: effects on neuronal discharge. *Biological Cybernetics, 30*, 115–123.

Tuckwell, H. C. (1988). *Introduction to Theoretical Neurobiology, vol. 2: Nonlinear and stochastic theories*. Cambridge: Cambridge Univ. Press.

Yamauchi, S., Kim, H., & Shinomoto, S. (2011). Elemental spiking neuron model for reproducing diverse firing patterns and predicting precise firing times. *Frontiers in Computational Neuroscience, 5*, 42.